Optimizing Surface-Enhanced Raman Spectroscopy Substrates with Gold Nanospheres, Nanorods and Nanostars

[1*]SANTACRUZ-GOMEZ K.J., [2]LÓPEZ DURAZO V.H, [3]GUTIÉRREZ FÉLIX S.J,[4]GUTIÉRREZ VELASQUEZ A.V, [5]ÁNGULO-MOLINA A.

ABSTRACT

Surface-Enhanced Raman Spectroscopy—is a powerful technique that boosts the distinctive fingerprint signals of molecules, making them more accessible for analysis. It utilizes metallic nanoparticles, acting as amplifiers, to greatly enhance the signals emitted by the molecules. This study aimed to explore the SERS potential of gold nanoparticles (AuNPs) with different geometries using a non-resonant molecule, 4-MBA. Nanospheres (14±2 nm), nanorods (11±2 nm x 50±7 nm) and nanostars (38±4 nm) were synthesized via the $HAuCl_4$ reduction method. All three AuNP geometries exhibited a remarkable enhancement of the Raman signal of 4-MBA by a magnitude of 10^4. Notably, only gold nanorods and nanostars displayed localized surface plasmon within the biological window, making them highly suitable for biological sample analysis. Meanwhile, the application of gold nanospheres should be limited to chemical SERS detection. These findings confirm the potential use of these nanostructures as SERS substrates for studying molecules with low molar absorption coefficients and low or zero quantum yield.

[1]Doctora en Ciencia de Materiales, Departamento de Física, Universidad de Sonora, Hermosillo, Sonora, México, karla.santacruz@unison.mx, https://orcid.org/0000-0002-5387-6482

[2]Q.B.C, Departamento de Ciencias Químico-Biológicas, Universidad de Sonora, Hermosillo, Sonora, México. victorh.lopezd1@gmail.com, https://orcid.org/0009-0005-0319-3690

[3]Estudiante de Q.B.C Departamento de Ciencias Químico Biológicas, Hermosillo, Sonora, México, a221205416@unison.mx, https://orcid.org/0009-0009-1752-8163

[4]Maestría en Ciencias de la Salud. Departamento de Ciencias Químico Biológicas, Hermosillo, Sonora, México, a215205849@unison.mx.

[5]Doctora en Ciencias, Departamento de Ciencias Químico-Biológicas, Universidad de Sonora, Hermosillo, Sonora, México aracely.angulo@unison.mx, https://orcid.org/0000-0002-8586-3387.

Autor de Correspondencia: Karla Santacruz Gómez, karla.santacruz@unison.mx

Cómo citar este artículo:

Santacruz-Gomez, K., López Durazo, V. H., Gutiérrez Félix, S. J., Gutiérrez Velázquez, A., & Ángulo-Molina, A. Optimizando sustratos de espectroscopía Raman mejorada en superficie con nanoesferas, nanorodillos y nanoestrellas de oro. EPISTEMUS, 17(35). https://doi.org/10.36790/epistemus.v17i35.315.
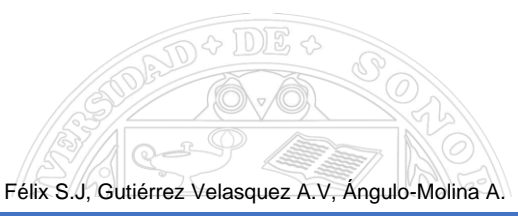
Optimizando sustratos de espectroscopía Raman mejorada en superficie con nanoesferas, nanorodillos y nanoestrellas de oro

RESUMEN

La Espectroscopía Raman Mejorada en Superficie es una potente técnica que realza las señales distintivas de huella dactilar de las moléculas, haciéndolas más accesibles para su análisis. Utiliza nanopartículas metálicas, que actúan como amplificadores para mejorar, en gran medida, las señales emitidas por las moléculas. Este estudio tuvo como objetivo explorar el potencial de SERS de nanopartículas de oro (AuNPs) con diferentes geometrías utilizando una molécula no resonante, el 4-MBA. Se sintetizaron nanoesferas (14 ± 2 nm), nanorrodillos (11 ± 2 nm x 50 ± 7 nm) y nanoestrellas (38 ± 4 nm) mediante el método de reducción de $HAuCl_4$. Las tres geometrías de AuNP mostraron una mejora notable en la señal Raman del 4-MBA en una magnitud de 10^4. Es importante destacar que solo los nanorrodillos y las nanoestrellas de oro presentaron resonancia de plasmón superficial localizada dentro de la ventana biológica, lo que las hace altamente adecuadas para el análisis de muestras biológicas. Mientras tanto, la aplicación de nanoesferas de oro debería limitarse a la detección química de SERS. Estos hallazgos confirman el potencial uso de estas nanoestructuras como sustratos de SERS para estudiar moléculas con coeficientes de absorción molar bajos y rendimiento cuántico bajo o nulo.

Palabras clave: *Nanoparticulas de oro, Plasmon de superficie localizado, SERS, moléculas no resonantes.*

INTRODUCTION

Spectroscopy encompasses a diverse range of techniques that analyze the interaction between light and materials, providing valuable insights into their properties based on its distinctive spectral fingerprint [1]. Among these methods, Raman technique is specialized in studying inelastic scattering. This occurs when light goes through a small change in energy due to its interaction with the vibrations of molecules, which acts as a unique identifier for the molecular composition of various substances, including both materials and biological samples [2]. However, its potential is constrained by the often weak signals generated during interactions with materials. This limitation, arising from infrequent inelastic scattering events, especially in complex or trace-level samples. To overcome this challenge, metallic nanoparticles have been used as signal amplifiers in a technique known as surface-enhanced Raman spectroscopy (SERS). With this technique, it is possible to achieve a signal amplification of up to 10^{11} times, enabling the detection of individual molecules [3]. The SERS effect arises from the intrinsic property of noble metallic nanoparticles, such as gold, known as localized surface plasmon resonance. It results in the collective oscillation of conduction electrons on the surface of the nanoparticle in resonance with the incident light producing changes in the surface electric field that enhance Raman scattering event [4]. The direct relationship between the size and shape of metallic nanoparticles and their localized surface plasmon (LSP) behavior is widely recognized [5]. These parameters can be precisely adjusted during the synthesis process, offering control over the plasmonic properties of the nanoparticles. As a result, numerous architectures of metallic nanoparticles have been extensively explored to assess the SERS potential, being exceptionally suitable anisotropic configurations [6]. In this context, the SERS enhancement factor (EF) serves as a quantifiable parameter that measures the amplification of

Raman signals by a substrate [7]. It is determined by comparing the Raman signals of non-resonant molecules in the presence and absence of the substrate, highlighting the substrate's effectiveness in enhancing the Raman scattering signal.

Here, 4-mercaptobenzoic acid (4-MBA) will be used as a probe molecule to determine the SERS efficiency of gold nanoparticles in three different geometries: nanospheres, nanorods and nanostars, and their EF will be reported.

METHODOLOGY

Gold nanoparticles were synthesized in three different configurations: spherical, rod-shaped, and star-shaped, using the CTAB-based reduction method. The process begins with seed nanoparticles formation, which serve as templates for growth all configurations, as described below.
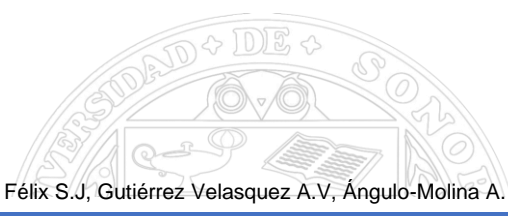
Gold seed synthesis

1.66 mL of a 0.2 M solution of cetyltrimethylammonium bromide (CTAB) were added to a glass vial. Subsequently, 1.84 mL of ultrapure water were added to bring the solution to the desired concentration. Then, 8 µL of a 0.1 M $HAuCl_4$ stock solution were added. Finally, 20 µL of freshly prepared cold $NaBH_4$ were added to obtain 3.528 mL of the seed solution.

Gold nanospheres

5 mL of a 0.08 M CTAB solution were prepared and then 13 µL of a 0.1 M $HAuCl_4$ stock solution, 28 µL of a 0.1 M ascorbic acid stock solution, and 500 µL of the previously prepared seed solution were added to obtain 5.54 mL of a gold nanosphere solution.

Gold nanorods

5 mL of a 0.2 M CTAB solution were added to a test tube. Then, 5.56 mL of ultrapure water were added to make a desired concentration solution. After that, 50 µL of a 0.1 M $HAuCl_4$ stock solution, 60 µL of a 0.01 M $AgNO_3$ stock solution, 55 µL of a 0.1 M ascorbic acid stock solution, and 12 µL of the previously prepared seed solution were added to obtain 10.23 mL of a gold nanorod solution.

Gold nanostars

2.38 mL of a 0.2 M CTAB solution were added to a test tube. Then, 2.56 mL of ultrapure water were included to achieve the required concentration. After that, 20 µL of a 0.1 M $HAuCl_4$ stock solution, 30 µL of a 0.01 M $AgNO_3$ stock solution, 32 µL of a 0.1 M ascorbic acid stock solution, and 10 µL of the previously prepared seed solution were added to obtain 5.02 mL of a gold nanostars solution.

UV-Vis spectroscopy

200 µL of the sample were placed in a well of a 96-well plate. Additionally, the Multiskan Go spectrophotometer from Thermo Scientific was used to measure from 300 nm to 900 nm at room temperature. The same procedure was performed for all samples.

Dynamic Light Scattering (DLS)

1 mL of a 1:5 diluted nanoparticle solution was placed in a disposable plastic cuvette. Then it was placed inside the Anton Paar Litesizer 500 instrument. The measurement conditions were lateral dispersion, room temperature (21.9 °C), 30 s equilibration time, general analysis model, ISO 22412 cumulant model, 6 runs processed with a duration of 10 s each, the filter optical density was 1.370, the focus position was -0.2 nm, the refractive index of the material was 0.6480, the absorbance

coefficient of the material was 3.2000, the solvent was water, the refractive index of the solvent was 1.3306, and finally the viscosity of the solvent was 0.9570 mPas.

Raman and SERS Microspectroscopy

For the Raman spectrum measurement of 4-MBA, a drop of a 10 mM solution of 4-MBA was placed on a CaF$_2$ Raman substrate and allowed to dry in the air. Then, the measurement was taken using a 532 nm laser. The Raman enhancement factor was determined as follows:

$$REF = \frac{I_{SERS}/N_{SERS}}{I_{REF}/N_{REF}} \tag{1}$$

$$N_{SERS} = \frac{(N \; x \; S_{NP})}{S_{mol}} \tag{2}$$

$$N_{Ref} = C \; x \; V_{eff} \; x \; N_A \tag{3}$$

RESULTS

Using the method described by Kozanoglu [8], we successfully synthesized a solution of gold seeds with an average diameter of 6±1 nm. The CTAB solution used in the process has a characteristic soapy appearance due to its surfactant nature, as shown in Figure 1. When gold is introduced, it forms an insoluble AuCl$_4$-CTA complex that can be observed as a yellowish precipitate in the tube. However, gentle agitation breaks the complex and turns the solution yellow (as seen in Fig. 1A). The addition of cold NaBH$_4$ to the solution leads to an instantaneous color change from yellow to brown, which is an indicator of successful gold seed synthesis.
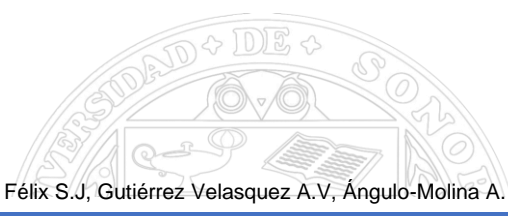
Similarly, gold nanospheres with a diameter of 14±2 nm (Fig. 2B), were obtained using the citrate reduction method [6]. In this case, both solutions initially appeared visually identical. Nevertheless, with the introduction of the seeds, the solution turned reddish rapidly to confirm the gold nanospheres formation [9, 10]. This transformation involves the reduction of gold ions, utilizing the gold seeds as nucleation sites, which subsequently promotes the growth of nanoparticles into spherical shapes, which can be controlled by fine-tuning the concentration of the gold seeds and adjusting reaction conditions, such as temperature and reaction time [11].

Additionally, we synthetized anisotropic gold nanoparticles such as nanorods and nanospheres. During gold nanorods synthesis, the surfactant and gold precursor were combined to form a yellowish solution. Upon the introduction of $AgNO_3$ to direct particle growth towards the desired geometry, no significant changes were observed in the solution. However, after the addition of ascorbic acid, the solution turns from a yellow to a colorless appearance, indicating the reduction of the gold complex. Although no immediate change was seen after adding the seeds, the solution gradually developed a fainted pink hue after about 5 minutes. Within 10 minutes, the pink color became clearly visible. Approximately 30 minutes after the addition of seeds, the solution acquired a dark purple hue, which was consistent with the desired nanorod geometry. In this process we obtained nanorods with transverse localized surface plasmon (LSP) dimensions of 11±2 nm and longitudinal LSP dimensions of 50±7 nm, as shown in Figure 2C.

Similar to other anisotropic geometries, the metamorphosis color was observed on the gold nanostars formation, but the final solution acquired a gray tone. As shown in Figure 2D, spherical nanoparticles with an average size of 38±4 nm, with spicules, were identified as nanostars.

Additionally, it was observed that the solution exhibited different colors when viewed from various angles due to light scattering. Thus, evidence of the presence of nanostars was proved[12].
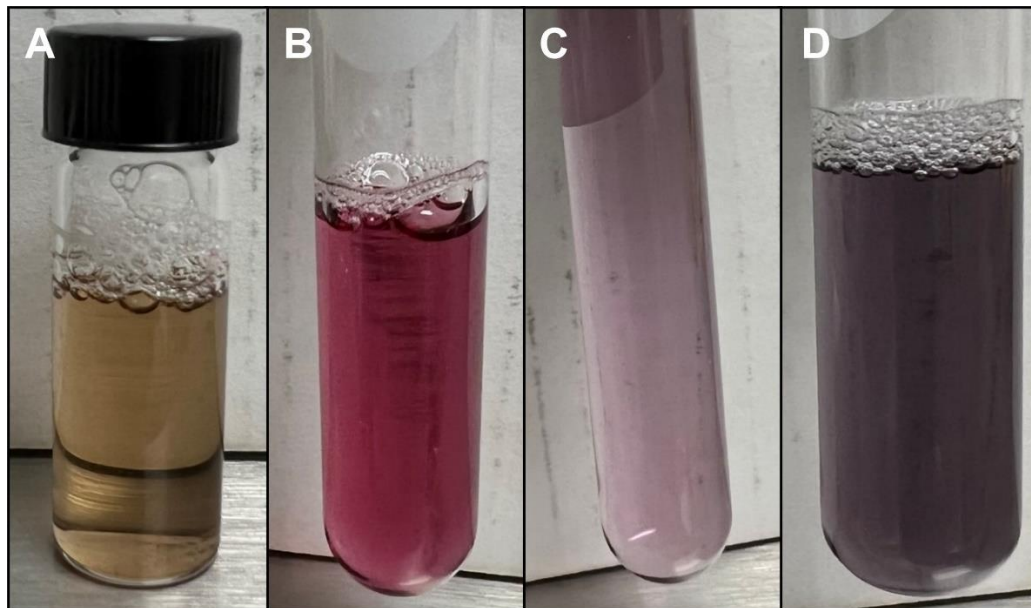

Figure 1. Appearance of the solutions of gold nanoparticles as A) seeds, B) nanospheres, C) nanorods, and D) nanostars.
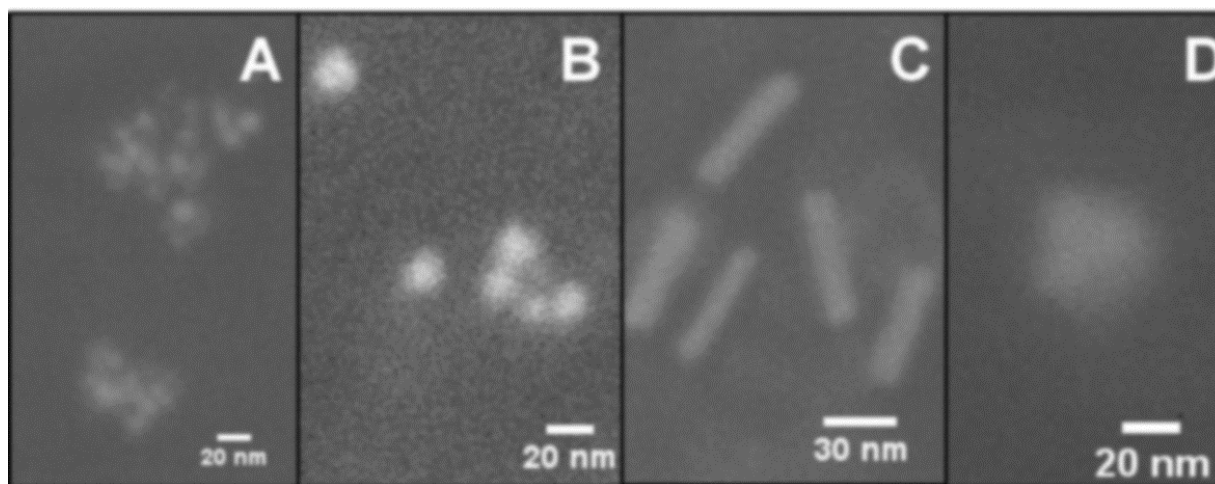

Figure 2. SEM images of gold nanoparticles with varying geometries: A) seeds, B) spheres, C) rods and D) stars.

Gold nanoparticles size in solution: Hydrodynamic size.

The hydrodynamic diameter is a measurement of the size of a particle in solution, which considers the influence of the surrounding solvent molecules and the Brownian motion of the particle. It is often determined by using techniques such as dynamic light scattering (DLS) or nanoparticle tracking analysis (NTA). The hydrodynamic diameter differs from the physical diameter, which only takes into account the solid part of the particle; it includes any adsorbed or solvated molecules on the particle surface, as well as any tendency for the particles to aggregate or cluster in the solution [13]. As a result, it provides a more precise measurement of the effective size of the particle in solution. This is important since it allows us to better understand how the particle behaves in solution, and how it may interact with other particles or biological systems.

Figure 3 displays the hydrodynamic size distribution results for the gold seed in water solution, which indicate an average size of 1 nm. However, the lack of surface stabilization on the seed may have caused particle aggregates to form. The gold nanospheres solution exhibited a narrow band with a peak located at 25 nm, along with a wider band at 164 nm, suggesting the presence of particle aggregates [14]. Similarly, the hydrodynamic size distribution of the nanorods and nanostars solutions indicated the presence of particle aggregates, as shown by larger and wider bands with a peak above the expected size range. It is important to note that the presence of particle aggregates can affect the interpretation of experimental results [15] and should be taken into consideration during further analysis.
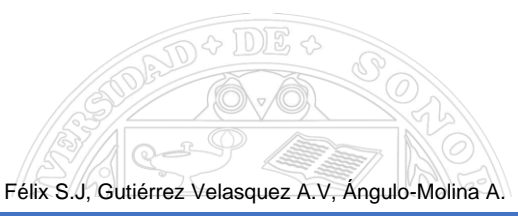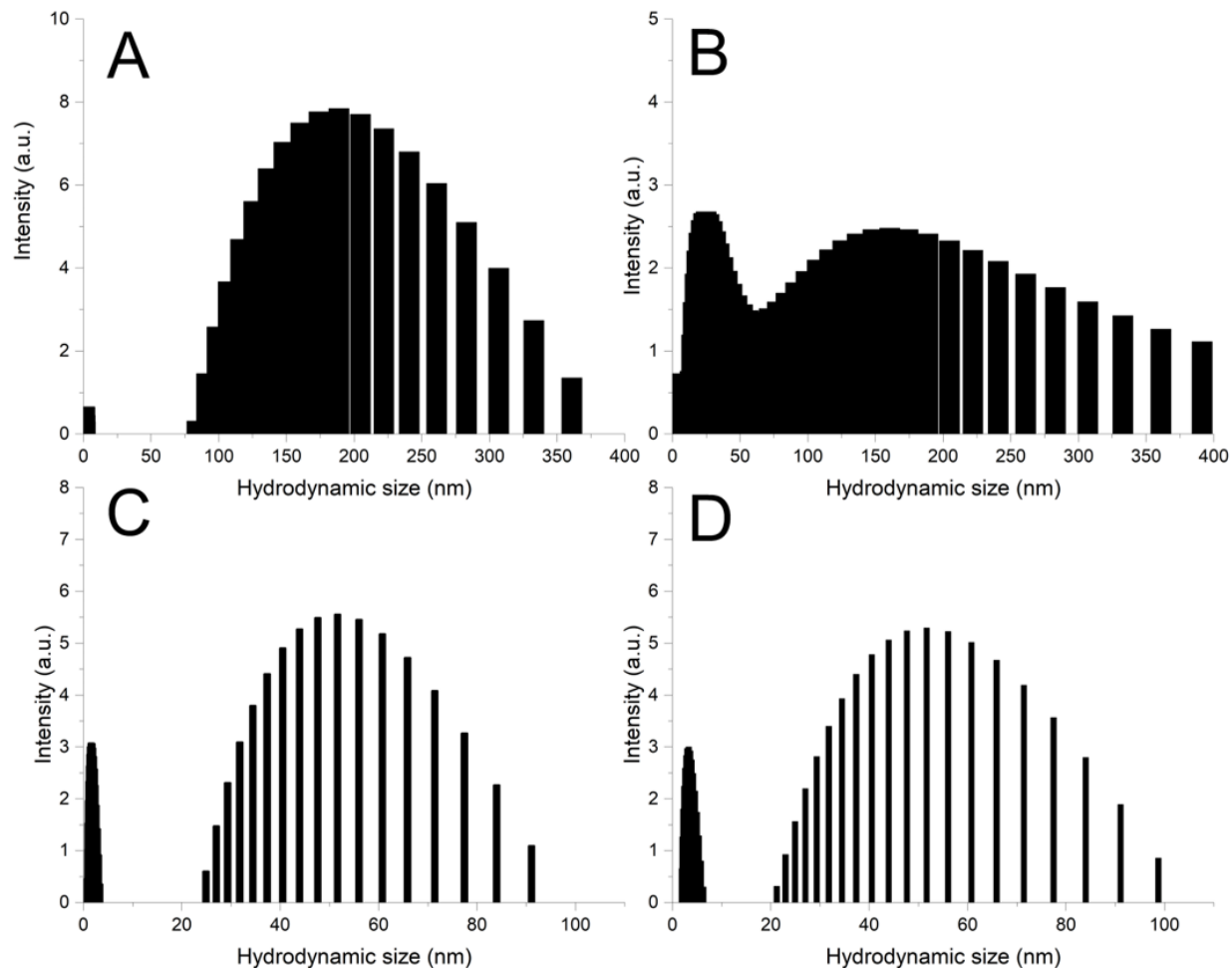
Figure 3. Hydrodynamic diameters of gold seeds (A), Nanospheres (B), Nanorods (C), and Nanostars (D).

Future work may require experimentation with different approaches to determine the most effective method for addressing the aggregation problem in this specific case. Techniques such as surface functionalization, ultrasonic treatment, centrifugation, or altering the synthesis method could be explored to minimize particle aggregation and obtain more accurate results [16].

The quantum effect of gold nanoparticles: localized surface plasmon

Colloidal gold exhibits one or multiple peaks of maximum absorption, representing the localized surface plasmon (LSP) associated with the specific shape of the gold particle [17]. The position and intensity of the plasmon resonance can be adjusted by varying the size, shape, and surrounding environment of the gold particles [5], making colloidal gold an attractive material for various applications in biomedical imaging, sensing, and therapy.

Figure 4 shows the absorption spectrum of gold nanoparticles with different geometries, indicating the LSP by using arrows. The absence of the 505 and 520 nm peaks in the optical spectrum [18] confirms the presence of genuine gold seed, as observed here. Therefore, the nanoparticles under investigation can be classified as gold seeds. Gold nanospheres are characterized by a broad absorption band with a maximum peak locates at about 526 nm, representing the LSP, which is consistent with literature reports for spherical gold nanoparticles with a size of about 20-30 nm. The shape of the absorption spectrum also indicates the monodispersity of the sample, with only one maximum corresponding to the LSP, indicating that the particles are of similar size and shape [19].

It can be observed in Figure 4 that the gold nanorods' absorbance spectrum comprises two bands. The first band, consistent with the transverse plasmon of a nanorod, has a maximum peak at 532 nm and is of a lower magnitude. The second band, closer to the infrared and of greater magnitude, has a maximum peak at 758 nm and is due to the longitudinal plasmon of the nanorods. This unique property of the nanorod is attributed to its location near the first biological window [20]. The presence of these two bands confirms the anisotropic shape of the particles as they have two different axes that generate different plasmonic resonances. For nanostars, the absorption

spectrum shows two distinct bands located at 532 and 809 nm, as well as a shoulder at 613 nm (Fig. 4). These shoulders are observed as minor peaks or bumps that appear on either side of the main absorption peak of the nanostars and can be attributed to their unique structural characteristics. Unlike spherical nanoparticles, nanostars possess anisotropic shapes with multiple sharp branches or tips. These branches create localized surface plasmon resonances (LSPR) that lead to enhanced electromagnetic field confinement and stronger light-matter interactions. However, unlike gold nanorods, nanostars do not have a well-defined absorption spectrum as it depends on various factors such as size, synthesis protocol, number of peaks and shape. The band with a maximum peak at 532 nm (Figure 4, blue line) is likely to belong to the core of the star, while the other two bands may belong to the plasmons of the star points. It is also possible that other geometries are present in the sample as the methods used for synthesizing nanostars can yield polydisperse results, which decreases monodispersity with increasing anisotropy. Therefore, this spectrum may represent the sum of overlapped types of nanostars. [21].

Anisotropic gold nanoparticles are more likely to exhibit LSP in the near-infrared radiation (NIR), which make them particularly interesting for bio applications such as SERS-based biosensing, imaging, and cancer therapy [22]. These capabilities extend to scenarios where gold nanoparticles are seamlessly integrated into nanocomposites, further broadening their potential application as needed [23, 24].
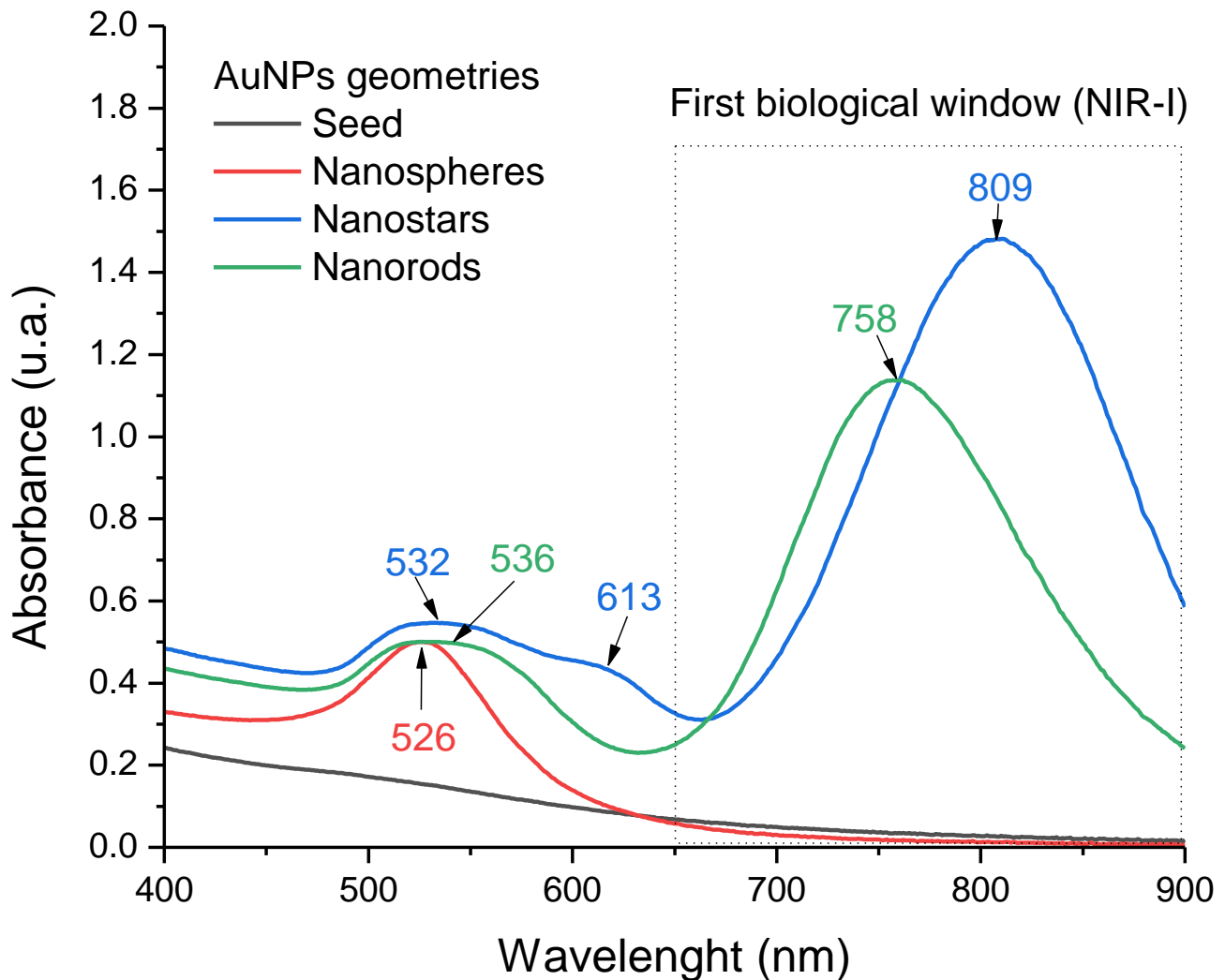
Figure 4. Absorbance spectrum of AuNPs of different geometries. The peaks of maximum absorption are indicated by the arrows, and they represent the LSP of the sample. The spectral region in which light can penetrate most deeply into biological tissue, known as the "biological window" (650-950 nm), is depicted by the dotted lines.

Table 1. Summary of the physical properties of the nanoparticles

Geometry	LSP (nm)	Size SEM (nm)	Hydrodynamic size (nm)
Seed	NA	6±1	1±1
Nanospheres	526	14±2	25±10
Nanorods	532 and 758	11±2 and 50±7	3±1 and 52±24
Nanostars	536, 613 and 809	38±4	2±1 and 51±19

Surface-Enhanced Raman Spectroscopy (SERS) for analyte detection

The SERS a powerful spectroscopic technique that amplifies the Raman signal of a molecule up to several orders of magnitude by placing the molecule in close proximity to a roughened metal surface or metal nanoparticle [25]. The Raman signal is enhanced because the molecule interacts with the localized electromagnetic field generated by the surface plasmon resonance of the metal substrate. This technique is highly sensitive and selective for the detection of small molecules and biological molecules due to the high enhancement factor. SERS has numerous potential applications in biomedical research, environmental monitoring, and chemical analysis due to its ability to detect low concentrations of analytes and provide detailed information about their chemical structure and environment.

Figure 5 illustrates the Raman spectrum of 4-MBA at a concentration of 10 mM, both with and without gold nanoparticles of various geometries. The inset provides a close-up view of a specific spectral region, which highlights a considerable amplification of the Raman signal for 4-MBA based on the shape of the gold nanoparticles. Table 2 facilitates the identification of the observed peaks and their corresponding molecule. The four peaks observed for 4-MBA are located at 1101, 1132, 1173, and 1600 cm^{-1}, while the six peaks for CTAB are located at 455, 760, 1278, 1300, 1140, and

1470 cm^{-1}. The peak at 1101 cm^{-1} for 4-MBA corresponds to the ring's "breathing" while the peak at 1600 cm^{-1} corresponds to the ring's stretching, both of which involve vibrational movements in the carbon-carbon bond [26]. Additionally, the peaks at 1132 and 1173 cm^{-1} correspond to the bending of the carbon-hydrogen bond. Concerning the CTAB molecule, the peak at 455 cm^{-1} corresponds to the deformation of C_4N^+, while the peak at 760 cm^{-1} corresponds to the stretching of CN^+. Furthermore, the peaks at 1278 and 1300 cm^{-1} correspond to the twisting and wagging of CH2, while the peaks at 1140 and 1470 cm^{-1} correspond to the scissoring motion of CH_2 and deformation of CH_3 [27]. The detection of characteristic peaks for both molecules at the same time demonstrates the ability of this technique to detect multiple analytes in a single measurement (multiplexing).
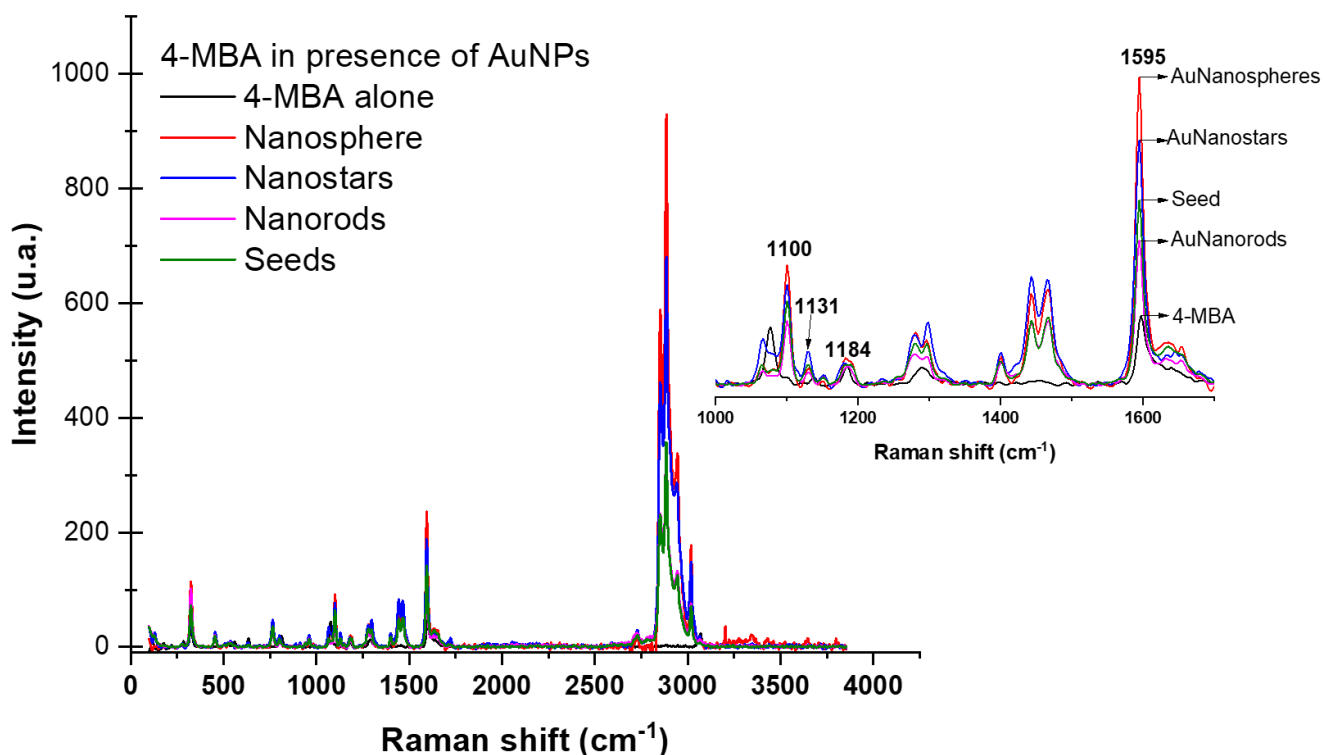
Figure 5. Raman spectrum of 4-MBA 10 mM in absence and in presence of gold nanoparticles with different geometries. The inset shows a particular region of the spectrum where a significant amplification of the Raman signal of 4-MBA is observed according to the gold nanoparticle shape.

Table 2. Maximum peaks of 4-MBA and CTAB in Raman

4-MBA (cm^{-1})	CTAB (cm^{-1})
1600 C_6H_6	1470 CH_3
1173 CH	1440 CH_2
1132 CH	1300 CH_2
1101 C_6H_6	1278 CH_2
	760 CN^+
	455 C_4N^+

The enhancement factor is a critical parameter for determining the SERS capabilities of nanoparticles, measuring the increase in Raman signal intensity when a molecule is adsorbed onto a plasmonic surface such as a metal nanoparticle [28]. The calculation entails dividing the SERS signal of the molecule (Raman reading in the presence of the substrate) by its value in a non-plasmonic context (conventional Raman measurement). Various factors influence the EF, including nanoparticle size, shape, and composition, excitation wavelength, and molecular properties of the analyte. By optimizing these factors, the sensitivity and detection capabilities of SERS can be improved, lowering the limit of detection of the analyte of interest. Here, we report the results of calculating the EF for the 4-MBA molecule, as described in the previous section, and present them in Table 3.
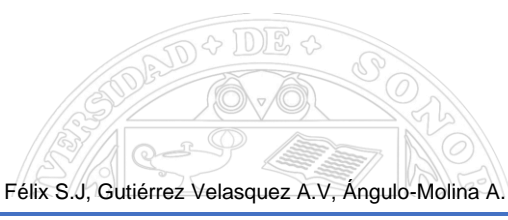
The EF is a crucial parameter in SERS because it determines the sensitivity of the technique. To calculate the EF values, we analyzed the 4-MBA molecule peaks at 1100.26 cm^{-1}, 1131.069 cm^{-1}, 1174.52 cm^{-1}, and 1594.474 cm^{-1} for each particle geometry and determined their average values. Our results showed that gold nanostars had the highest average EF at 2.5×10^4, followed by gold nanospheres with a high average EF of 2.0×10^4. Meanwhile, gold seeds had the lowest average EF at 1.7×10^4, and gold nanorods had an intermediate average EF of 1.2×10^4. These findings indicate that the particle shape plays a crucial role in enhancing the Raman signal of 4-MBA, with gold nanostars and nanospheres exhibiting higher efficiency than gold seeds and nanorods [20].

Furthermore, as reported in the reference [29], we anticipated that gold nanostars would demonstrate the highest EF due to the intense Raman signals generated by the electrons confined at the tips of anisotropic nanoparticles, analogous to hot spots. The average EF value for gold nanostars is consistent with reported values, confirming their potential as excellent SERS substrates. However, the branched shape of gold nanostars also presents some drawbacks, including the polydispersity obtained with conventional methods and the intricate functionalization of the nanoparticle surface due to its curved shape.

The confirmation that both gold nanorods and nanostars synthesized in this study are capable of significantly enhancing the Raman spectra of non-resonant molecules, such as 4-MBA, by 10^4, is of great relevance. This finding confirms the possibility of employing these nanostructures as SERS substrates for evaluating molecules with low molar absorption coefficients and low or zero quantum yield.

Lastly, it is important to emphasize that regardless of the gold nanoparticles' architecture, the biocompatibility of these particles often requires specific treatments to be addressed, hence improving their suitability for diverse bio applications [30].

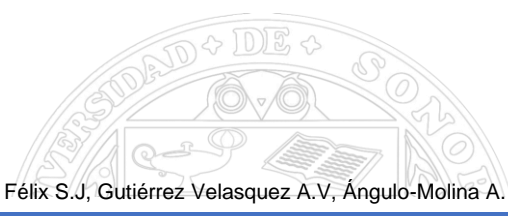**Table 3. Enhancement factor associated to nanoparticles.**

Raman Shift (cm^{-1})	1100 (x10^4)	1131 (x10^4)	1184 (x10^3)	1595 (x10^3)	Average (x10^4)
Seed	2.8	2.7	6.2	6.9	1.7
Nanospheres	4.0	2.3	5.8	12.0	2.0
Nanorods	2.1	1.6	4.6	5.4	1.2
Nanostars	3.4	4.5	1.1	9.1	2.5

CONCLUSIONS

In this study, we synthesized three different colloidal gold nanoparticle geometries: spheres, rods, and stars, and investigated their potential as SERS substrates. Our findings successfully demonstrate that these nanoparticles enhance the Raman spectra of mercaptobenzoic acid (4-MBA), a non-resonant molecule, with enhancement factors ranging from 10^3 to 10^4. This significant result further highlights the applicability of our gold nanostructures as SERS substrates for a wide range of molecules, particularly those with limited optical properties.

Furthermore, considering that the anisotropic shapes (such as nanorods and nanostars) exhibit LSP within the biological window and display the highest SERS amplification efficiency, they are considered the most suitable candidates for bio-applications. On the other hand, nanospheres are recommended for detecting other types of analytes, such as chemical SERS applications.
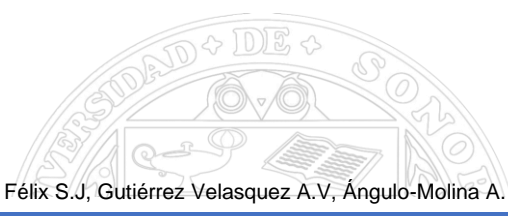
REFERENCES

[1]   S. Agnello, *Spectroscopy for Materials Characterization* (no. 1). Wiley Online Library, 2021.

[2]   E. C. Le Ru, E. Blackie, M. Meyer, and P. G. Etchegoin, "Surface enhanced Raman scattering enhancement factors: a comprehensive study," *J. Phys. Chem. C J,* vol. 111, no. 37, pp. 13794-13803, 2007.

[3]   S. Zeng *et al.*, "Size dependence of Au NP-enhanced surface plasmon resonance based on differential phase measurement," *Sens. Actuators B: Chem.,* vol. 176, pp. 1128-1133, 2013.

[4]   L. Jiang *et al.*, "Surface-enhanced Raman scattering spectra of adsorbates on Cu 2 O nanospheres: charge-transfer and electromagnetic enhancement," *Nanoscale* vol. 5, no. 7, pp. 2784-2789, 2013.

[5]   S. Liu, G. Chen, P. N. Prasad, and M. T. J. C. o. M. Swihart, "Synthesis of monodisperse Au, Ag, and Au–Ag alloy nanoparticles with tunable size and surface plasmon resonance frequency," *ACS Appl Mater Interfaces,* vol. 23, no. 18, pp. 4098-4101, 2011.

[6]   J. Reguera, J. Langer, D. Jimenez de Aberasturi, and L. M. Liz-Marzan, "Anisotropic metal nanoparticles for surface enhanced Raman scattering," *Chem Soc Rev,* vol. 46, no. 13, pp. 3866-3885, Jul 3 2017.

[7]   E. Le Ru, M. Meyer, E. Blackie, and P. Etchegoin, "Advanced aspects of electromagnetic SERS enhancement factors at a hot spot," *J Raman Spectrosc* vol. 39, no. 9, pp. 1127-1134, 2008.

[8]   E. Kooij, W. Ahmed, C. Hellenthal, H. Zandvliet, and B. Poelsema, "From nanorods to nanostars: Tuning the optical properties of gold nanoparticles," *Colloids Surf. A Physicochem.,* vol. 413, pp. 231-238, 2012.

[9]   A. L. Siegel and G. A. Baker, "Bespoke nanostars: synthetic strategies, tactics, and uses of tailored branched gold nanoparticles," *Nanoscale Adv,* vol. 3, no. 14, pp. 3980-4004, Jul 13 2021.

[10]   I. Blakey, Z. Merican, and K. J. Thurecht, "A method for controlling the aggregation of gold nanoparticles: tuning of optical and spectroscopic properties," *Langmuir,* vol. 29, no. 26, pp. 8266-74, Jul 2 2013.

[11]   R. Fenger, E. Fertitta, H. Kirmse, A. F. Thunemann, and K. Rademann, "Size dependent catalysis with CTAB-stabilized gold nanoparticles," *Phys Chem Chem Phys,* vol. 14, no. 26, pp. 9343-9, Jul 14 2012.

[12]   L. Fabris, "Gold nanostars in biology and medicine: understanding physicochemical properties to broaden applicability," *J. Phys. Chem. C J,* vol. 124, no. 49, pp. 26540-26553, 2020.

[13]   A. Jillavenkatesa, S. J. Dapkunas, and L.-S. H. Lum, *Particle size characterization* (no. 960). National Institute of Standards and Technology, 2001.

[14]   O. C. Compton and F. E. Osterloh, "Evolution of size and shape in the colloidal crystallization of gold nanoparticles," *J Am Chem Soc,* vol. 129, no. 25, pp. 7793-8, Jun 27 2007.

[15]   W. Zhang, "Nanoparticle aggregation: principles and modeling," *Adv Exp Med Biol,* vol. 811, pp. 19-43, 2014.

[16]   J. Amaro-Gahete *et al.,* "A Comparative Study of Particle Size Distribution of Graphene Nanosheets Synthesized by an Ultrasound-Assisted Method," *Nanomaterials (Basel),* vol. 9, no. 2, p. 152, Jan 26 2019.

[17]   S. Szunerits, J. Spadavecchia, and R. J. R. i. A. C. Boukherroub, "Surface plasmon resonance: Signal amplification using colloidal gold nanoparticles for enhanced sensitivity," *Rev Anal Chem,* vol. 33, no. 3, pp. 153-164, 2014.

[18]   S. Picciolini, D. Mehn, I. Ojea-Jimenez, F. Gramatica, and C. Morasso, "Hydroquinone Based Synthesis of Gold Nanorods," *J Vis Exp,* no. 114, p. e54319, Aug 10 2016.

[19]   C. G. Khoury and T. Vo-Dinh, "Gold Nanostars For Surface-Enhanced Raman Scattering: Synthesis, Characterization and Optimization," *J Phys Chem C Nanomater Interfaces,* vol. 2008, no. 112, pp. 18849-18859, 2008.

[20]   E. Hemmer, A. Benayas, F. Legare, and F. Vetrone, "Exploiting the biological windows: current perspectives on fluorescent bioprobes emitting above 1000 nm," *Nanoscale Horiz,* vol. 1, no. 3, pp. 168-184, May 25 2016.

[21]   O. Bibikova *et al.*, "Surface enhanced infrared absorption spectroscopy based on gold nanostars and spherical nanoparticles," *Anal Chim Acta,* vol. 990, pp. 141-149, Oct 16 2017.

[22]   C. Kohout, C. Santi, and L. Polito, "Anisotropic Gold Nanoparticles in Biomedical Applications," *Int J Mol Sci,* vol. 19, no. 11, p. 3385, Oct 29 2018.

[23]   W. Janetanakit *et al.*, "Gold-Embedded Hollow Silica Nanogolf Balls for Imaging and Photothermal Therapy," *ACS Appl Mater Interfaces,* vol. 9, no. 33, pp. 27533-27543, Aug 23 2017.

[24]   A. H. Mo *et al.*, "Dual-Functionalized Theranostic Nanocarriers," *ACS Appl Mater Interfaces,* vol. 8, no. 23, pp. 14740-6, Jun 15 2016.

[25]   B. Sharma, R. R. Frontiera, A.-I. Henry, E. Ringe, and R. P. J. M. t. Van Duyne, "SERS: Materials, applications, and the future," *Mater Today,* vol. 15, no. 1-2, pp. 16-25, 2012.

[26]   C. J. Orendorff, A. Gole, T. K. Sau, and C. J. Murphy, "Surface-enhanced Raman spectroscopy of self-assembled monolayers: sandwich architecture and nanoparticle shape dependence," *Anal Chem,* vol. 77, no. 10, pp. 3261-6, May 15 2005.

[27]   A. Dendramis, E. Schwinn, and R. Sperline, "A surface-enhanced Raman scattering study of CTAB adsorption on copper," *J. Phys. Chem. C J,* vol. 134, no. 3, pp. 675-688, 1983.

[28]   E. Le Ru, M. Meyer, E. Blackie, P. J. J. o. R. S. A. I. J. f. O. W. i. a. A. o. R. S. Etchegoin, Including Higher Order Processes,, a. Brillouin, and R. Scattering, "Advanced aspects of electromagnetic SERS enhancement factors at a hot spot," *J Raman Spectrosc* vol. 39, no. 9, pp. 1127-1134, 2008.

[29]   A. Sabur, M. Havel, and Y. Gogotsi, "SERS intensity optimization by controlling the size and shape of faceted gold nanoparticles," vol. 39, no. 1, pp. 61-67, 2008.

[30]   K. Santacruz-Gomez, R. Melendrez, M. Licerio-Ramírez, A. L. Gallego-Hernandez, M. Pedroza-Montero, and R. J. J. o. N. R. Lal, "Alterations on HeLa cell actin filaments induced by PEGylated gold nanorod-based plasmonic photothermal therapy," *J Nanopart Res* vol. 24, no. 2, p. 38, 2022.